

# The flow of an Oldroyd fluid past a reentrant corner: the downstream boundary layer

J.M. Rallison\*, E.J. Hinch

*Department of Applied Mathematics and Theoretical Physics, Centre for Mathematical Sciences,  
University of Cambridge, Wilberforce Road, Cambridge CB3 0WA, UK*

Received 10 August 2003; received in revised form 3 October 2003

---

## Abstract

We reconsider the steady planar flow of an Oldroyd-B fluid within a small distance  $r$  of a sharp reentrant corner of angle  $\pi/p$ ,  $1/2 \leq p < 1$ . Previous theoretical studies of this problem have been unable to resolve a boundary layer near the downstream wall. For a range of angles  $\pi/p$ , including the benchmark problem  $p = 2/3$ , and for several non-zero solvent viscosities, we have solved the equations for the downstream boundary layer numerically and additionally found asymptotic results for a frozen stress limit and for high solvent viscosities. For each angle and viscosity we find a one-parameter family of attached ‘potential’ flows, for each of which the stress is proportional to  $r^{2p-2}$  and the velocity proportional to  $r^{p(3-p)-1}$  as proposed by Hinch [J. Non-Newtonian Fluid Mech. 50 (1993) 161]. The limiting member of the family has zero shear stress on the upstream wall. The stress is that of a purely elastic neo-Hookean solid in the interior of the flow, with boundary layers on both the upstream and downstream walls having the similarity structure proposed by Renardy [J. Non-Newtonian Fluid Mech. 58 (1995) 83]. The behaviour of these flows is discussed. We propose a form of elastic Kutta condition to determine the separation angle for flows having an upstream lip vortex.

© 2003 Elsevier B.V. All rights reserved.

*Keywords:* Corner flow; Oldroyd-B fluid; neo-Hookean solid; Boundary layer; Lip vortex; Separation

---

## 1. Introduction

The nature of the flow of a viscoelastic fluid near a sharp reentrant corner is of fundamental interest. Stress singularities at corners arise in computations and, if the local corner structure is understood, may be removed by means of an appropriate singular element. For an elastic liquid, the failure to resolve the stress adequately near a corner may pollute the stress downstream. The primary aim of this paper is to take forward the studies of the problem by Hinch [3] and Renardy [7]. Hinch’s paper suggested a flow having a stress that is purely elastic but, as pointed out by Renardy, fails in boundary layers near the walls.

---

\* Corresponding author. Tel.: +44-223-337912.

E-mail address: j.m.rallison@damtp.cam.ac.uk (J.M. Rallison).

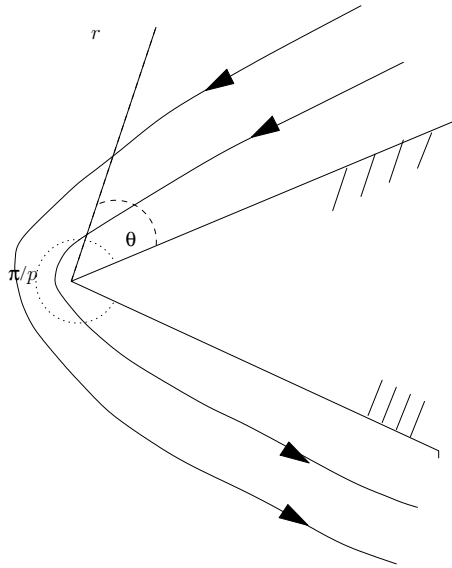


Fig. 1. Sketch of the flow geometry.

Renardy provided a family of solutions for the upstream layer, but did not obtain converged numerical solutions for the downstream layer, leaving open the possibility that no solution of the kind sought exists. We begin by offering a summary of, and different perspective on, these earlier contributions.

### 1.1. The flow geometry

We shall assume that the flow does not separate at the corner. The flow is then as sketched in Fig. 1. In consequence, every material particle that reaches the corner originated from the viscometric region close to the upstream wall.

Since the residence time of particles near this no-slip wall is long, the upstream boundary condition on the elastic stress is provided by this viscometric region: any earlier flow history is forgotten. For a flow that separates on either the upstream or downstream sides of the corner, additional upstream stress information is needed.

Within a small radius  $r$  of the corner, the steady fluid velocity, proportional to  $r^k$  for some  $k$  with  $0 < k < 1$ , is small. Fluid inertia is therefore unimportant, and the stress  $\sigma$  is such that  $\nabla \cdot \sigma = 0$ .

On the other hand, the velocity gradient, which scales as  $r^{k-1}$ , is large. Thus; if the fluid relaxation time is  $\tau$ , the local Weissenberg number  $Wi = \tau|\nabla\mathbf{u}|$  is large. Furthermore, the time rate-of-change of  $\nabla\mathbf{u}$  as seen by a material particle gives a Deborah number  $De = \tau|\mathbf{u} \cdot \nabla\mathbf{u}|/|\mathbf{u}|$ , and, with the exception of shear-flow regions near the walls where  $\mathbf{u} = 0$ ,  $De$  is also large. It follows that away from these boundary layers, the material has the constitutive response of a non-linear purely elastic solid, for the instantaneous viscous stress proves to be negligible. The structure of the different flow regions is sketched in Fig. 2.

The stress is given in terms of a polymer strain tensor  $\mathbf{A}$ , an elastic modulus  $G_e$  and a solvent viscosity  $\mu_0$ , as

$$\sigma = -PI + 2\mu_0\mathbf{E} + G_e\mathbf{A}, \quad (1)$$

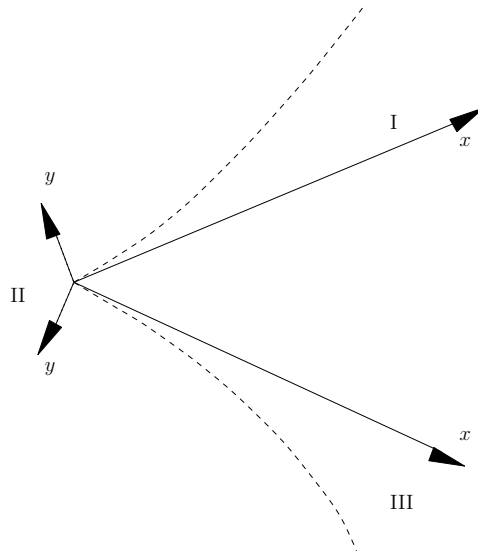


Fig. 2. Sketch of the different flow regions: (I) the upstream boundary layer; (II) the interior elastic core; (III) the downstream boundary layer. Local Cartesian coordinates for the boundary layers are shown.

where  $P$  is the pressure. For a steady flow,

$$\mathbf{u} \cdot \nabla \mathbf{A} = \mathbf{A} \cdot \nabla \mathbf{u} + \nabla \mathbf{u}^T \cdot \mathbf{A} - \frac{1}{\tau}(\mathbf{A} - \mathbf{I}). \tag{2}$$

Rescaling lengths with respect to some fixed scale  $a$ , times with respect to  $\tau$ , velocities with respect to  $a/\tau$  and stresses with respect to  $G_e$ , we may set  $\tau = 1$  and  $G_e = 1$ , and then the only parameter apart from  $p$  needed to describe the flow near the corner is  $\mu_0/G_e\tau$  which, for convenience, we call  $\mu_s$ . We then replace  $\mu_0$  by  $\mu_s$  in Eq. (2) above. The case  $\mu_s = 0$  represents a Maxwell fluid. We anticipate that a similarity solution for the flow near the corner will not depend upon the choice of the scale  $a$ .

We now discuss the different flow regions separately.

### 1.2. The elastic core

For a sufficiently strong fast flow with  $Wi \rightarrow \infty$  and  $De \rightarrow \infty$ , the relaxation term is negligible, and the dominant balance in (2) is

$$\mathbf{u} \cdot \nabla \mathbf{A} = \mathbf{A} \cdot \nabla \mathbf{u} + \nabla \mathbf{u}^T \cdot \mathbf{A}.$$

This equation gives the constitutive behaviour of a neo-Hookean solid, because  $\mathbf{A}$  represents the affine rotation and stretching of material line elements in the flow. As noted by Renardy [6], it is helpful for steady planar flows to write the solution of this equation in the form

$$\mathbf{A} = \lambda \mathbf{u} \mathbf{u} + \frac{\mu(\mathbf{u} \mathbf{u}_\perp + \mathbf{u}_\perp \mathbf{u})}{|\mathbf{u}|^2} + \frac{\nu \mathbf{u}_\perp \mathbf{u}_\perp}{|\mathbf{u}|^4}, \tag{3}$$

where  $\mathbf{u}_\perp = \mathbf{e}_z \times \mathbf{u}$ . When there is no stress relaxation, the coefficients  $\lambda$ ,  $\mu$  and  $\nu$  are constants on each streamline, and thus depend only on the streamfunction  $\psi$ .

Outside the boundary layers, the fluid velocity increases along streamlines as the corner is approached (even though the velocity is zero at the corner). As a result, the dominant term in the stress near the corner is the first, so that

$$\mathbf{A} = \lambda(\psi)\mathbf{u}\mathbf{u}.$$

Because  $\lambda^{1/2}|\mathbf{u}|$  represents the stretch of a material line element that starts and remains parallel to  $\mathbf{u}$ , the coefficient  $\lambda$  can never vanish, and must remain positive.

Near the corner we assume provisionally that this elastic stress  $\mathbf{A}$  is asymptotically larger than the viscous stress  $2\mu_s\mathbf{E}$ . This assumption is verified a posteriori; it implies that the limit  $\mu_s = \infty$  for which the fluid is Newtonian, and for which the Moffatt corner flow obtains [4], is singular. The momentum equation  $\nabla \cdot \boldsymbol{\sigma} = 0$  then gives an Euler equation

$$\lambda^{1/2}\mathbf{u} \cdot \nabla(\lambda^{1/2}\mathbf{u}) = \nabla P,$$

for the unknown ‘velocity’  $\lambda^{1/2}\mathbf{u}$ . Furthermore, this ‘flow’ is incompressible since

$$\nabla \cdot (\lambda^{1/2}\mathbf{u}) = \mathbf{u} \cdot \nabla \lambda^{1/2} = 0.$$

We can therefore find the pressure  $P$  from a Bernoulli theorem for the energy flux along the steady streamlines that

$$\lambda^{1/2}\mathbf{u} \cdot \nabla(P - w) = 0,$$

where  $w = \frac{1}{2}\lambda\mathbf{u}^2$  is the dominant term in the elastic energy density of this neo-Hookean material. The pressure thus increases along streamlines wherever  $\lambda^{1/2}|\mathbf{u}|$  increases (of opposite sign to the inertial Bernoulli effect).

Now the Euler equation admits potential flow solutions with

$$\lambda^{1/2}\mathbf{u} = \nabla\phi \quad \text{and} \quad \nabla^2\phi = 0,$$

and in that case the pressure is given everywhere as

$$P = \frac{1}{2}\lambda\mathbf{u}^2.$$

For a reentrant corner, a solution having  $u_\theta = 0$  on the walls  $\theta = 0$  and  $\theta = \pi/p$  is

$$\phi \propto r^p \cos(p\theta),$$

for which the stress is proportional to  $r^{2p-2}$ . The corresponding pressure is (surprisingly) independent of  $\theta$  and increases as the corner is approached. The physical effect of the pressure gradient is thus to increase the magnitude of the wall shear rate on the downstream side of the corner, but to reduce it on the upstream side. We might therefore expect, and indeed will find, that for a given pressure gradient, there is a critical flow rate on the upstream side at which the flow reverses and separation occurs.

Other potential flow solutions satisfying these boundary conditions are available, but no other describes a flow that remains attached to the upstream and downstream walls. It remains an open question whether non-potential solutions of the Euler equation can be found to match to the upstream and downstream stresses and flows. It would be possible to add a small perturbation term having  $\phi \propto r^{mp} \cos np\theta$  for integer  $n$ , but we have not pursued such corrections.

### 1.3. Matching

We now turn to the upstream wall-layer where the Deborah number is not large. Within this layer the fluid velocity is parallel to the wall at leading order, and so the flow is a simple shear having shear rate  $\dot{\gamma}(x)$ . In Cartesian coordinates we have  $\mathbf{u} = (\dot{\gamma}y, 0)$  with corresponding streamfunction (at leading order)  $\psi = \frac{1}{2}\dot{\gamma}y^2$ . The largest stress component is the normal stress  $\sigma_{xx}$  proportional to  $\dot{\gamma}^2$ . In order that this should match the stress in the outer elastic region when  $r = x$ , we must have  $\dot{\gamma} \propto x^{p-1}$ . The shear rate thus increases without bound as the corner is approached.

The Deborah number may then be calculated as

$$De = \frac{|\mathbf{u} \cdot \nabla \mathbf{u}| \tau}{|\mathbf{u}|} \propto yx^{p-2} = \xi.$$

In the absence of any other length-scale, the dynamics within the boundary layer are controlled by a similarity variable,  $\xi$ , (having the significance of a Deborah number), as proposed by Renardy [7].

We have still to match this upstream flow to that in the interior so as to determine  $\lambda^{1/2}(\psi)$ . This matching must take place where the Deborah number is of order unity, i.e. where  $y \propto x^{2-p}$  so that  $\psi \propto x^{3-p}$ , giving a fluid velocity  $u \propto x$ . In order that the stress,  $\lambda \mathbf{u}^2$ , at this location is proportional to  $x^{2p-2}$ , it must be the case that  $\lambda^{1/2} \propto x^{p-2}$ , giving

$$\lambda^{1/2} \propto \psi^{(p-2)/(3-p)}.$$

From our result for  $\lambda^{1/2} \mathbf{u}$  we may finally determine  $\psi$  itself in the core as

$$\psi = Cr^{p(3-p)} \sin^{3-p}(p\theta), \tag{4}$$

where  $C$  is a constant. For the attached flow sketched in Fig. 1,  $C < 0$ . The exponent of  $r$  varies from  $5/4$  when  $p = 1/2$ , to  $2$  when  $p = 1$ , confirming our expectations that  $\mathbf{u} \rightarrow 0$  and  $\nabla \mathbf{u} \rightarrow \infty$  as  $r \rightarrow 0$ . We note too that the level of viscous stress in the elastic region is  $\mu_s r^{p(3-p)-2}$ , and this is negligible as  $r \rightarrow 0$  compared with the elastic stress,  $r^{2p-2}$  as assumed.

At this stage, the eigenvalue in the problem (the exponent of  $r$ ) has been fixed by the choice of potential flow in the elastic region; the boundary layers near  $\theta = 0$  and  $\theta = \pi/p$  have still to be determined. The problem has features in common with high-Reynolds-number Newtonian flow past a wedge, where viscous boundary layers governed by the Falkner–Skan equation arise near the walls. In both problems, the outer flow has stresses that are quadratic in the steady fluid velocity (though with a sign change here); such a stress cannot be consistent with the no-slip condition at the wall, and in consequence viscous effects must become important in a boundary layer on the wall. The question is whether any solution of the boundary layer equations exists that remains attached to the walls; for if the flow detaches, the nature of the upstream stress boundary condition is changed, and the entire solution procedure described above fails.

### 1.4. The boundary layers

We now consider the boundary layers in detail. For definiteness, we focus on the upstream layer near  $\theta = 0$ , but by relabelling axes so that the downstream wall is defined by  $y = 0, x > 0$  as shown in Fig. 2, both layers satisfy the same governing equations. Note, however, that for a right-handed set of axes, the sense of  $\mathbf{e}_z$ , and hence  $\mathbf{u}_\perp$  in (3), is different for the upstream and downstream layers.

Within the boundary layer, a similarity variable (in fact the Deborah number)  $\xi = y/x^{2-p}$  has already been identified. The streamfunction may be written

$$\psi = x^q \chi(\xi),$$

for some  $q$  and some function  $\chi$  to be determined. If this is to match the exterior flow (4) when  $\theta = y/x \rightarrow 0$  and  $r = x$  we must have,

$$\chi \rightarrow C\xi^{3-p} \quad \text{as } \xi \rightarrow \infty, \quad \text{and } q = 3 - p.$$

The Cartesian velocity components are then

$$u = x\tilde{u}(\xi) \quad \text{and} \quad v = x^{2-p}\tilde{v}(\xi),$$

confirming that  $u \gg v$  as  $x \rightarrow 0$ , where

$$\tilde{u} = \chi' \quad \text{and} \quad \tilde{v} = (p-3)\chi + (2-p)\xi\chi'.$$

The velocity gradients are

$$\begin{aligned} \frac{\partial u}{\partial x} &= -\frac{\partial v}{\partial y} = \chi' - (2-p)\xi\chi'', & \frac{\partial u}{\partial y} &= x^{p-1}\chi'', \\ \frac{\partial v}{\partial x} &= x^{1-p}[(3-p)(2-p)(\xi\chi' - \chi) - (2-p)^2\xi^2\chi'']. \end{aligned}$$

Because the polymer stress,  $\mathbf{A}$ , has the form  $\lambda\mathbf{u}\mathbf{u}$  in the outer flow, its scaling with  $x$  is known. Following Renardy [7] we therefore write

$$\mathbf{A} - \mathbf{I} = \begin{pmatrix} x^{2p-2}f(\xi) & x^{p-1}g(\xi) \\ x^{p-1}g(\xi) & h(\xi) \end{pmatrix}. \quad (5)$$

The functions  $f$ ,  $g$  and  $h$  are then related to the stress coefficients  $\lambda$ ,  $\mu$  and  $\nu$  in (3) by

$$f = \lambda\tilde{u}^2, \quad g = \lambda\tilde{u}\tilde{v} + \mu \quad \text{and} \quad h = \lambda\tilde{v}^2 + \frac{2\mu\tilde{v}}{\tilde{u}} + \frac{\nu}{\tilde{u}^2} - 1, \quad (6)$$

with inverse relationships

$$\lambda = \frac{f}{\tilde{u}^2}, \quad \mu = g - \frac{f\tilde{u}}{\tilde{v}} \quad \text{and} \quad \nu = (1+h)\tilde{u}^2 + f\tilde{v}^2 - 2g\tilde{u}\tilde{v}. \quad (7)$$

Substituting into the governing equation (2) for the Oldroyd fluid gives

$$(p-3)\chi f' = (4-2p)[\chi' - \xi\chi'']f + 2\chi''g - f, \quad (8)$$

$$(p-3)\chi g' = (1-p)\chi'g + (2-p)[(3-p)(\xi\chi' - \chi) - (2-p)\xi^2\chi'']f + \chi''h - g + \chi'', \quad (9)$$

$$\begin{aligned} (p-3)\chi h' &= 2(2-p)[(3-p)(\xi\chi' - \chi) - (2-p)\xi^2\chi'']g \\ &\quad + 2[-\chi' + (2-p)\xi\chi'']h - h + 2[-\chi' + (2-p)\xi\chi'']. \end{aligned} \quad (10)$$

We now turn to the momentum equation. Because the boundary layer is thin, the leading order pressure across it is uniform, and only the  $x$ -component of the momentum need be considered. The magnitude of

the pressure gradient is determined (by Bernoulli) in the outer elastic region, whose stress scaling ( $x^{2p-2}$ ) we have already found. We write for the far-field

$$P = \frac{1}{2}\lambda\mathbf{u}^2 = \frac{Gx^{2p-2}}{2p-2},$$

and then the pressure gradient throughout the boundary layer is  $Gx^{2p-3}$ . Because the pressure is highest at  $x = 0$  we require that  $G < 0$ .

The momentum equation becomes

$$\mu_s\chi''' + (2p-2)f - (2-p)\xi f' + g' = G. \tag{11}$$

Eqs. (8)–(11) were obtained by Renardy [7] for the case  $p = 2/3$ .

Although the equations for both boundary layers are the same, the boundary conditions are not. For the upstream layer, at  $\xi = 0$  there is no slip and so  $\chi = \chi' = 0$ . The shear rate  $\chi''_u(0)$  on the upstream wall is unknown, but it fixes the initial values at  $\xi = 0$  of  $f$ ,  $g$  and  $h$  as  $f = 2[\chi''_u(0)]^2$ ,  $g = \chi''_u(0)$  and  $h = 0$ .

As  $\xi \rightarrow \infty$  we must match to the outer solution so  $\chi \rightarrow C\xi^{3-p}$ . We shall also need the behaviour of the stress variables since these provide an upstream condition for the downstream layer. Although the parts of the stress represented in (3) by  $\mu$  and  $\nu$  are negligible in the elastic core, they are significant in both boundary layers, so conditions on  $\lambda$ ,  $\mu$  and  $\nu$  are needed. We have already seen that  $\lambda \propto x^{2p-4}$ ; similar arguments give  $\mu \propto x^{p-1}$  and  $\nu \propto x^2$ . Now  $\lambda$ ,  $\mu$  and  $\nu$  depend asymptotically only on  $\psi$  and it follows that as  $\xi \rightarrow \infty$ ,

$$\lambda \rightarrow \lambda^*|\chi|^{2(p-2)/(3-p)}, \quad \mu \rightarrow \mu^*|\chi|^{-(1-p)/(3-p)} \quad \text{and} \quad \nu \rightarrow \nu^*|\chi|^{2/(3-p)}, \tag{12}$$

where  $\lambda^*$ ,  $\mu^*$  and  $\nu^*$  are constants. These expressions for  $\lambda$ ,  $\mu$  and  $\nu$ , and the corresponding values of  $f$ ,  $g$ ,  $h$  derived from (6) exactly satisfy the stress evolution equations (8)–(10) for any streamfunction  $\chi(\xi)$ , provided the relaxation terms are neglected, which is certainly the case if  $\chi' \gg 1$ . They are therefore the *frozen stress* levels appropriate to a neo-Hookean solid.

We note for future reference that the momentum equation (11) with these far-field values gives, with errors of magnitude  $\xi^{-(2-p)}$  arising from the omission of relaxation terms,

$$\mu_s\chi''' - \lambda^*|\chi|^{(2p-4)/(3-p)}[(3-p)\chi\chi'' - (\chi')^2] = G. \tag{13}$$

We refer to this important result as the *frozen stress momentum equation*. Taking the limit  $\xi \rightarrow \infty$ , we find that  $\lambda^*$  may be inferred from  $C$  or vice versa as

$$\lambda^* = \frac{-G|C|^{-2/(3-p)}}{[(1-p)(3-p)^2]}. \tag{14}$$

We now consider the boundary conditions for the downstream layer. At the wall we must again have  $\chi = \chi' = 0$ . Far from the wall, the flow is reversed relative to that upstream and so  $\chi \rightarrow -C\xi^{3-p}$  as  $\xi \rightarrow \infty$ . The upstream conditions on the stress variables inherited from the upstream layer are applied as  $\xi \rightarrow \infty$ . Noting the reversal of sign of  $\mathbf{u}_\perp$  in (3) for the downstream layer we have

$$\lambda \rightarrow \lambda^*\chi^{2(p-2)/(3-p)}, \quad \mu \rightarrow -\mu^*\chi^{-(1-p)/(3-p)} \quad \text{and} \quad \nu \rightarrow \nu^*\chi^{2/(3-p)}.$$

As indicated in Fig. 1, we require that the velocity  $\chi'$  should be one-signed for each layer so that the upstream stress boundary condition is unmodified.

These equations and boundary conditions are invariant to a rescaling having the form

$$\begin{aligned} \xi &\rightarrow k\xi, & \chi &\rightarrow k\chi, & \tilde{u} &\rightarrow \tilde{u}, & \tilde{v} &\rightarrow k\tilde{v}, & f &\rightarrow k^{-2}f, & g &\rightarrow k^{-1}g, & h &\rightarrow h, \\ \lambda &\rightarrow k^{-2}\lambda, & \mu &\rightarrow k^{-1}\mu, & v &\rightarrow v, & G &\rightarrow k^{-2}G, & C &\rightarrow k^{p-2}C, \end{aligned}$$

for any constant  $k$ . Such a rescaling is equivalent to making a different choice for the reference length-scale  $a$ . We may use this freedom to fix  $G$  and determine  $C$ , or vice versa. Here we set  $G = -(1 - p)$ . In effect, then, the stress near the corner is prescribed, and the task is to determine (if any such solution exists) the corresponding amplitude,  $C$ , of the singular streamfunction.

Renardy [7] has considered the upstream boundary layer in isolation from that downstream. With an assumed value for  $\chi_u''(0)$ , and a Taylor series for the first step, it is possible to integrate the equations numerically away from the wall and to determine the flow for all values of  $\xi$ . We have repeated Renardy's calculations (for  $p = 2/3$ ), and our answers agree with his to three significant figures. Surprisingly, perhaps, *all* choices of  $\chi_u''(0) < 0$  are consistent with the far-field stress and velocity conditions (for a value of  $C$  that depends on  $\chi_u''(0)$ ). Thus this layer does not uniquely determine  $C$ . We note also that the stress variables attain their frozen levels when  $\xi_\infty = 10$ . The dynamics for  $\xi_\infty > 10$  are therefore controlled by the frozen stress equation (13).

The ambiguity of solutions for the upstream boundary layer arises because the outer elastic region is controlled, in part, by the upstream stress distribution. With our normalisation of the flow, the stress level  $\lambda u^2$  in the outer region is fixed. So if  $C$  and thus  $u$  are reduced, then  $\lambda^{1/2}$  must rise. But  $\lambda^{1/2}$  is determined by matching with the upstream boundary layer at the point in the flow where the Deborah number is of order unity. By increasing the magnitude of the wall stress  $\chi_u''(0)$  this matching takes place closer to the wall, and hence, since  $u$  is lower, brings about the required increase in  $\lambda^{1/2}$ . We quantify this effect below.

The downstream layer is vital to complete the problem. Renardy finds that a numerical integration away from the downstream wall is unstable. An alternative strategy for solving the downstream layer is needed which we consider in the next section.

## 2. The downstream boundary layer

### 2.1. A model problem

In order to understand the behaviour of the downstream layer we start with a model one-dimensional problem. Consider the differential equation

$$\mu_s \frac{du}{d\xi} - \lambda u^2 = G\xi, \tag{15}$$

where  $\lambda$  is a positive constant, and  $G$  a negative constant. We seek a solution in  $\xi \geq 0$  such that  $u$  remains bounded and one-signed for all finite  $\xi$ . An equation of this kind would arise, after one integration, for pressure-driven flow of a fluid having viscous stress  $\mu_s du/d\xi$  and elastic stress  $-\lambda u^2$ . The model problem is closely related to the frozen stress momentum equation (13).

The solution trajectories for (15) for different initial conditions  $u(0)$  are sketched in Fig. 3. We see that on the upstream side, ( $u < 0$ ), all initial conditions provide a solution and lead to the same asymptotic behaviour  $u \sim -(-G\xi/\lambda)^{1/2}$  as  $\xi \rightarrow \infty$ . A one-parameter family of upstream solutions is thus available, exactly as Renardy found for the corner flow.

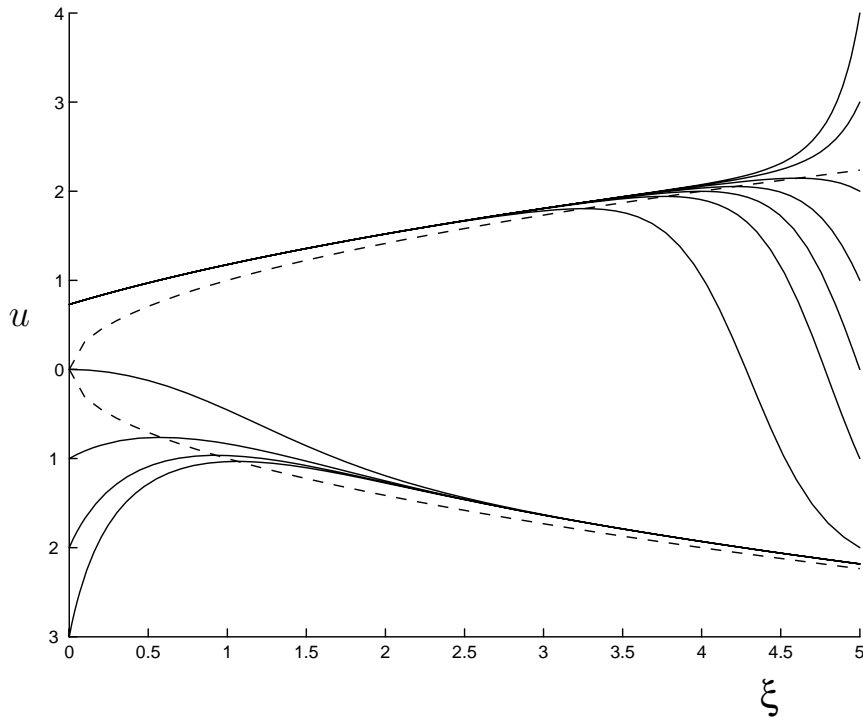


Fig. 3. Continuous curves show solution trajectories for the model equation (15) with  $\mu_s = \lambda = 1$ ;  $G = -1$ . Dotted lines indicate the asymptotic solutions  $u \sim \pm \xi^{1/2}$  downstream and upstream, respectively. Note that trajectories diverge from the downstream solution but converge to the upstream solution as  $\xi \rightarrow \infty$ .

On the downstream side ( $u > 0$ ), however, all trajectories except one either become negative, or unbounded, at some finite  $\xi$ . We conclude that there is a unique solution to the problem on the downstream side. This flow could be obtained numerically by shooting inward from  $\xi = \infty$  but not by shooting outward from  $\xi = 0$  because neighbouring trajectories move away from the solution. For the same reason, the solution for which  $u = (-G\xi_\infty/\lambda)^{1/2}$  at some finite  $\xi_\infty$  does not have the required behaviour  $u \sim (-G\xi/\lambda)^{1/2}$  as  $\xi \rightarrow \infty$ , so the far boundary condition is better expressed for numerical purposes in some other form.

We shall find that these behaviours for the upstream and downstream boundary layers arise in our full problem. We note too that the Maxwell limit  $\mu_s = 0$  is singular for this problem.

### 2.2. Reformulation of the equations

We have introduced two sets of stress variables:  $(\lambda, \mu, \nu)$  which provide the most convenient representation of the boundary conditions at  $\xi = \infty$ , and  $(f, g, h)$  which are more appropriate for the wall boundary conditions, together with transformations (6) and (7) that relate them. Unfortunately, neither set is wholly numerically satisfactory for the full range of  $\xi$ : the trouble is that  $\lambda$  becomes unbounded near the wall, whereas the task of obtaining  $\nu$  from  $f, g, h$  using (7) involves subtracting relatively large quantities. A compromise choice of stress variables that avoids these difficulties is

to write

$$l(\xi) = \lambda(\xi)(\chi')^2, \quad m(\xi) = \mu(\xi) \quad \text{and} \quad n(\xi) = \frac{v(\xi)}{(\chi')^2}. \quad (16)$$

The governing equations (8)–(10) become:

$$(3-p)\chi l' = \left[ 2(3-p)\frac{\chi\chi''}{\chi'} - 2(2-p)\chi' + 1 \right] l - 2\chi''m, \quad (17)$$

$$(3-p)\chi m' = [(p-1)\chi' + 1]m - \chi''n, \quad (18)$$

$$(3-p)\chi n' = \left[ -2(3-p)\frac{\chi\chi''}{\chi'} + 2\chi' + 1 \right] n - 1, \quad (19)$$

and the momentum equation is

$$\mu_s\chi''' - \frac{(3-p)\chi l'}{\chi'} + \frac{(3-p)\chi\chi''l}{(\chi')^2} - (3-2p)l + m' + (1-p) = 0. \quad (20)$$

In terms of these variables the boundary conditions become: on both walls  $\chi = \chi' = 0$ ; near the upstream wall for small  $\xi$ ,

$$l = 2[\chi_u''(0)]^2 \left[ 1 + 3(1-p)\xi\chi_u''(0) + \frac{2\chi_u'''(0)\xi}{\chi_u''(0)} \right],$$

$$m = \chi_u''(0) \left[ 1 + 2(1-p)\xi\chi_u''(0) + \frac{\chi_u'''(0)\xi}{\chi_u''(0)} \right], \quad n = 1 + (1-p)\xi\chi_u''(0),$$

and

$$\chi_u'''(0) = -\frac{(1-p)(1 + [\chi_u''(0)]^2)}{(1 + \mu_s)};$$

at infinity,  $\chi \rightarrow \pm C\xi^{3-p}$ , and

$$\frac{l|\chi|^{(4-2p)/(3-p)}}{(\chi')^2} \rightarrow \lambda^*; \quad m|\chi|^{(1-p)/(3-p)} \rightarrow \mp\mu^*; \quad n(\chi')^2|\chi|^{-2/(3-p)} \rightarrow v^*,$$

the signs being taken, respectively for the upstream and downstream layers.

### 2.3. Numerical method

There are two distinct reasons why an attempt to integrate the downstream boundary layer away from the wall  $\xi = 0$  fails.

The first reason concerns the stress equations. Near the wall,  $\chi \propto \xi^2$ . In consequence, as we show explicitly in Section 3, the quasi-linear stress evolution equations (17)–(19) have an essential singularity at  $\xi = 0$  with solutions for the stress variables that decay like  $\exp(-1/\xi)$  as the wall is approached. The corresponding solutions for the upstream layer behave as  $\exp(+1/\xi)$  and must be rejected, so it is possible there to take the first step away from the wall using a polynomial expansion, but this is not permissible on

the downstream side. On the other hand, if the streamfunction  $\chi(\xi)$  is known (and is everywhere positive) then it is permissible to integrate the stress equation *toward* the wall on the downstream side.

The second reason that an outward integration fails concerns the far-field momentum equation. We have already seen for the model problem (15) that all nearby trajectories depart from the correct solution as  $\xi$  increases. This behaviour persists for the frozen stress momentum equation (13). The solution that we want has  $\chi = -C\xi^{3-p}$  as  $\xi \rightarrow \infty$ . Three linearly independent infinitesimal perturbations to this solution may be found, two of which decay relative to the desired solution as  $\xi \rightarrow \infty$ , but the third grows at a rate  $\exp(-C\xi^p/\mu_s)$ , and this will pollute any numerical solution. On the upstream side with  $C < 0$ , all three linear perturbations decay away from the wall and thus a shooting method is successful. The difficulties arising from this growing perturbation evidently increase as the viscosity parameter  $\mu_s$  is reduced, or as the numerical range of  $\xi$  is increased. We conclude that even if the stresses are known exactly, the momentum equation cannot be integrated to infinity away from the wall. Nor, indeed, can it be integrated from infinity toward the wall (because the two benign perturbations grow in the opposite direction).

For a range of  $\xi$  smaller than  $\xi_\infty = 20$ , and with a viscosity  $\mu_s > 5$  and  $p = 2/3$  it is possible to contain the exponential growth and obtain converged solutions for the downstream layer using a Picard iteration. The stresses are integrated toward the wall, and the momentum equation away from the wall with a fixed velocity  $\chi' = -7C\xi_\infty^{4/3}/3$  imposed at  $\xi = \xi_\infty$ . But for smaller viscosities, even an under-relaxed Picard iteration converges very slowly (or perhaps not at all).

We found two more effective techniques. The first method is to introduce a simultaneous relaxation of the stress and streamfunction by means of a pseudo-time  $t$ . Assuming for a moment that the streamfunction,  $\chi(\xi)$ , is known, the stresses may be obtained either by integrating  $l$ ,  $m$  and  $n$  inward from their known asymptotic values imposed at  $\xi_\infty = 20$ , or else by a relaxation procedure with Eq. (17), for example, being replaced by

$$\frac{\partial l}{\partial t} = -(3 - p)\chi \frac{\partial l}{\partial \xi} + F_1(\xi),$$

where  $F_1$  is the right-hand side of (17), and with up-winding to solve the resulting advection equation.

Now assuming that the stresses are known, the momentum equation (20) may be written as a diffusion equation for the velocity  $\tilde{u} = \chi'$  as

$$\frac{\partial \tilde{u}}{\partial t} = \mu_s \frac{\partial^2 \tilde{u}}{\partial \xi^2} + F_2(\xi),$$

where  $F_2(\xi)$  is known, and with boundary conditions  $\tilde{u}(0) = 0$  and  $\tilde{u}(\xi_\infty)$  prescribed. This diffusion equation may be efficiently solved by a fully-implicit forward differencing scheme that is unconditionally stable in time so that large time steps may be taken (of course the accuracy of the time-stepping is irrelevant, since only a steady state is sought). In order to resolve both the near- and far-wall behaviours, we found it convenient to use a spatial grid having step-sizes increasing in geometric ratio away from the wall. Starting from a guessed profile for  $\tilde{u}(\xi)$ , for example the upstream flow profile, we found it necessary to *partially* relax the stresses and then recompute the velocity. A full relaxation was liable to generate reversed flows for which the stress equations become numerically unstable. Furthermore a full relaxation effectively gives a Picard iteration which is much slower to converge.

For the downstream layer, the relaxation procedure yields a steady converged solution. Only one downstream wall shear rate is consistent with the requirement that  $\chi' \propto \xi^{4/3}$  as  $\xi \rightarrow \infty$ ; for the wrong

choices of far-field velocity, the solution near  $\xi_\infty$  is contaminated by a growing exponential, so there is a unique satisfactory choice for  $\tilde{u}(\xi_\infty)$ .

During the numerical relaxation, successive iterates explore nearby trajectories, and these can involve wide excursions. It is important therefore to start close to the correct solution, for example by parameter continuation in  $p$ ,  $\mu_s$ ,  $C$  or  $\xi_\infty$ .

As  $\xi_\infty$  is increased, Eq. (13) implies that the satisfactory velocities  $\tilde{u}(\xi_\infty)$  automatically satisfy

$$\tilde{u}(\xi_\infty) \rightarrow -(3 - p)C\xi_\infty^{2-p},$$

where the value of  $C$  is set by  $\lambda^*$  through Eq. (14). Thus; the downstream layer does not select any value for  $C$ ; each choice of  $C$  determines a downstream layer. As found by Renardy for the upstream layer, there is a one-parameter family of solutions, labelled by  $C$ , to the entire problem, and thus the full parameter space of solutions is determined for each  $p$  by  $\mu_s$  and  $C$ .

We were able to reproduce these results for  $\chi(\xi)$  using the ‘black-box’ relaxation method `bvp4c` in MATLAB. By imposing the far-field boundary condition in the form  $\chi'(\xi_\infty) = (4/3)\chi(\xi_\infty)/\xi_\infty$  it is possible to avoid specifying the value of  $C$  or  $\tilde{u}(\xi_\infty)$ , and we could obtain converged solutions up to  $\xi_\infty = 100$  for  $\mu_s = 1$ . As with the time-relaxation method, it is vital to start from a good approximation to the correct solution otherwise the method fails to converge. Obtaining solutions becomes progressively more difficult as  $\mu_s$  is reduced.

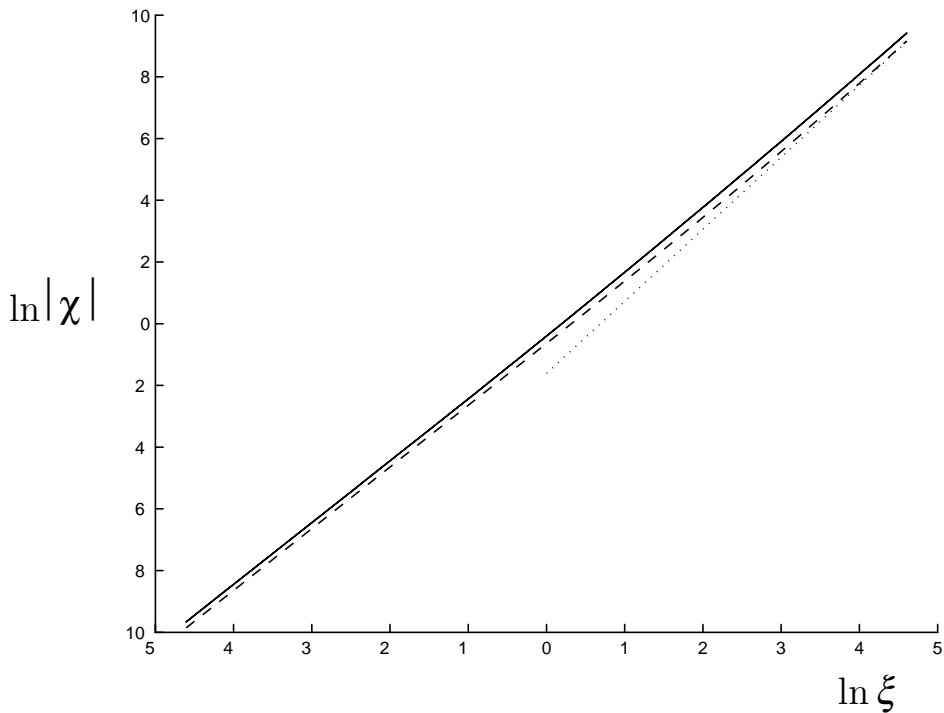


Fig. 4. Values of  $|\chi(\xi)|$  (log–log plot) for  $\chi''_u(0) = -1.05$ ,  $\mu_s = 1$  and  $p = 2/3$  for which  $C = -0.2$ . The dashed curve is the upstream boundary layer, the continuous curve the downstream layer, and the dotted curve the asymptote  $|C|\xi^{7/3}$ .

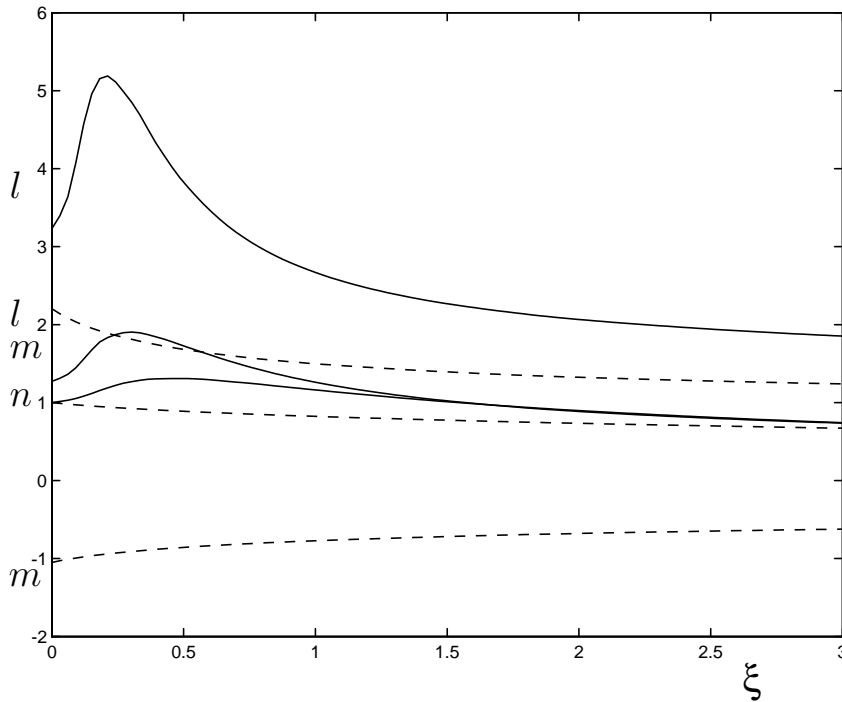


Fig. 5. Values of stress variables  $l$ ,  $m$  and  $n$  near the walls for  $\chi_u''(0) = -1.05$ ,  $\mu_s = 1$ ,  $p = 2/3$  for which  $C = -0.2$ . Dashed curves correspond to the upstream boundary layer, continuous curves to the downstream layer.

Both methods may be tested by using them for the upstream layer (except that  $\chi_u''(0)$  must also be prescribed so as to provide wall values for  $l$ ,  $m$  and  $n$ ), and compared with an easier shooting method. The results agree to within numerical accuracy, but the relaxation methods become very slow as the value of  $\xi_\infty$  is increased.

We show in Fig. 4 converged solutions for  $\chi(\xi)$  for the case  $p = 2/3$ ,  $\mu_s = 1$  and  $C = -0.2$  corresponding to  $\chi_u''(0) = -1.05$ . For  $\xi \rightarrow 0$ , the slope (on a log–log plot) is 2; for  $\xi \rightarrow \infty$  it is  $7/3$ . The corresponding stress variables  $l$ ,  $m$  and  $n$  near the walls are shown in Fig. 5. Note the pile up of elastic stresses convected away from the corner that relax as the downstream wall is approached. Stresses further from the wall normalised by their frozen values are shown in Fig. 6. The frozen level for  $l$  is attained in  $\xi > 10$ .

In order to make sense of the rather large parameter space involving  $C$ ,  $\mu_s$  and  $p$  it is possible to derive some scaling relationships as investigated below.

### 3. Some asymptotic results

#### 3.1. Behaviour of the frozen stress equation

We first consider the outer part of the boundary layers in which the stresses have attained their asymptotic levels (12), and are no longer relaxing. Thus; the flow is governed by the frozen stress equation (13),

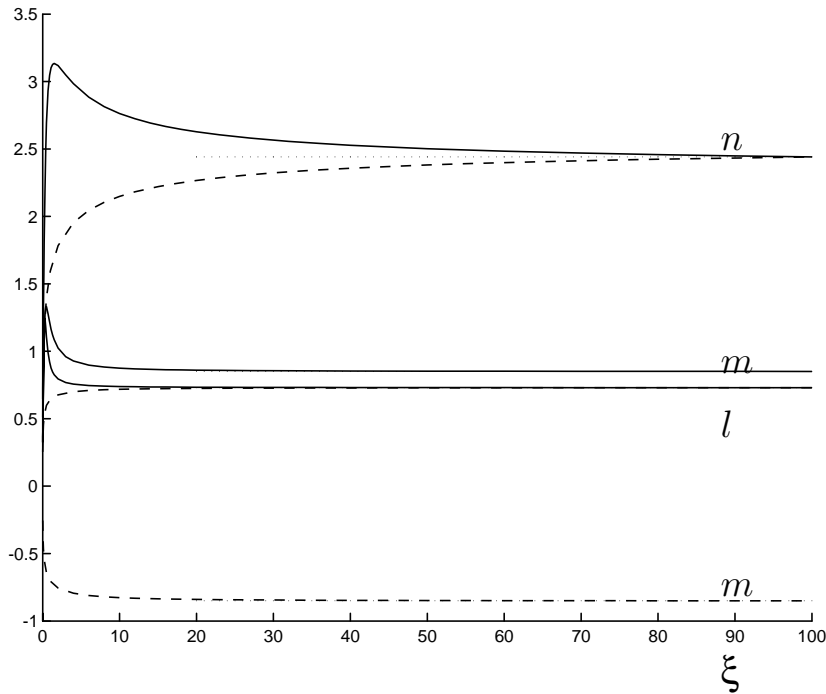


Fig. 6. Values of stress variables  $l|\chi|^{8/7}/|\chi'|^2$ ,  $m|\chi|^{1/7}$  and  $n|\chi'|^2/|\chi|^{6/7}$  far from the walls for  $\chi''_u(0) = -1.05$ ,  $\mu_s = 1$ ,  $p = 2/3$  for which  $C = -0.2$ . The dashed curves correspond to the upstream boundary layer, the continuous curves to the downstream layer. Asymptotic levels (shown dotted) are  $\lambda^* = 0.73$ ,  $\pm\mu^* = 0.85$  and  $v^* = 2.44$ . Note that this level is attained for  $l$  by  $\xi \sim 10$ .

which may be written

$$\mu_s \chi''' - |C|^{-2/(3-p)} |\chi|^{(2p-4)/(3-p)} \frac{[(3-p)\chi\chi'' - (\chi')^2]}{(3-p)^2} = -(1-p),$$

with asymptotic solution  $\chi \rightarrow \pm C\xi^{3-p}$ . Both  $C$  and  $\mu_s$  may be removed from the equation and boundary condition by writing

$$\chi(\xi) = \frac{(\mu_s|C|)^{3/p}}{\mu_s} \hat{\chi} \left[ \frac{\xi}{(\mu_s|C|)^{1/p}} \right], \tag{21}$$

for some master function  $\hat{\chi}$  that is the solution of the problem for which  $\mu_s$  and  $|C|$  are both unity. For the downstream layer, this scaling of the numerical results with  $C$  is effective, with collapsed data shown for several values of  $C$  in Fig. 7. Although the frozen stress equation applies only in the region far from the wall where  $\chi'' \gg 1$  for which the stress variables no longer relax, the collapse is remarkably good even in the near-wall region where stress relaxation occurs. Eq. (21) suggests on this basis that the downstream wall shear rate  $\chi''_d(0)$  is proportional to  $|C|^{1/p}$ .

The same data reduction is inappropriate for the upstream layer. The difficulty is that the value of  $\chi''_u(0)$  enters the boundary conditions, but it does not satisfy the same scaling behaviour (21) as the frozen stress equation.

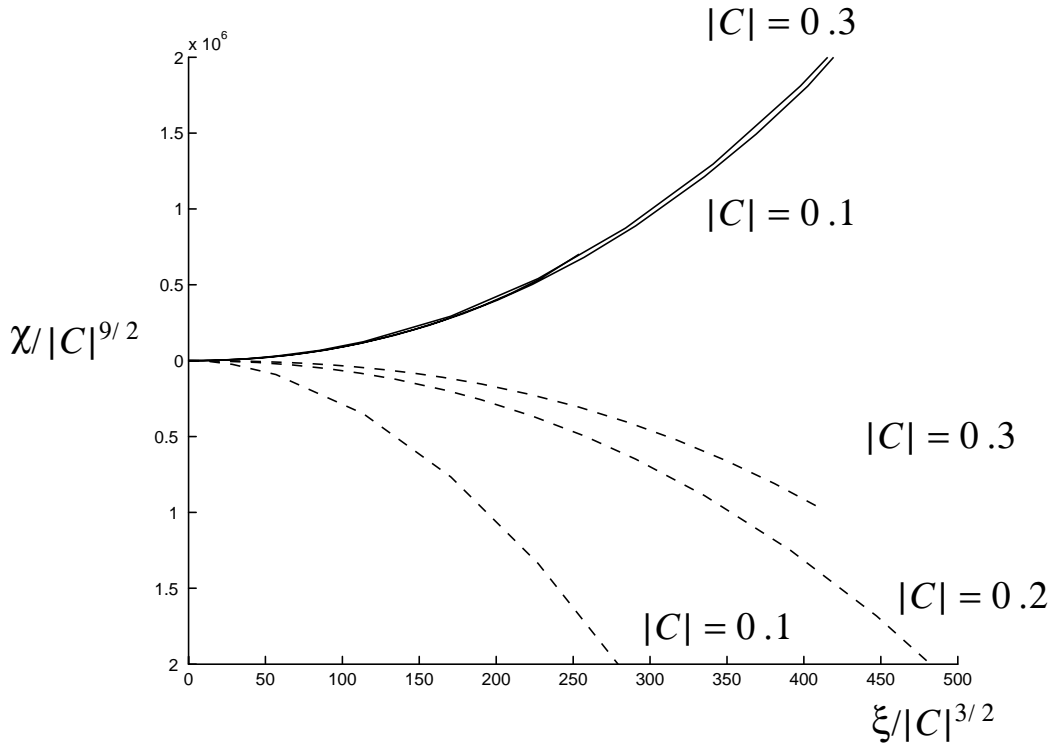


Fig. 7. Streamfunction  $\chi/|C|^{9/2}$  as a function of  $\xi/|C|^{3/2}$  for  $p = 2/3$ ,  $\mu_s = 1$  and values of  $C$  as shown. Continuous curves show the downstream layer; dashed curves are the upstream layer. The downstream curves are almost indistinguishable on this scale.

In Fig. 8 we show similar data for three values of  $\mu_s$ . If  $\mu_s > 1$ , the collapse for the downstream data works well, but if  $\mu_s < 1$  it is ineffective. Once again, and for the same reason given above, this scaling is inappropriate for the upstream layer.

### 3.2. Evolution of the stresses within the boundary layers

In Section 3.1 we considered solutions of the momentum equation (11) when the flow was sufficiently strong that the stresses did not relax. In this section we consider solutions to the stress Eqs. (8)–(11) in which stress relaxation plays an important role.

For a fluid having  $\mu_s \gg 1$ , the wall boundary layers become highly viscous so that  $\chi''' = 0$ , and thus the simple shear velocity profile near the wall extends throughout a significant part of the boundary layer. In consequence on the upstream side, the stresses can attain their frozen values (12) within the simple shear region, with subsequent adjustment of the flow profile taking place by Eq. (13). In this limit it is possible to derive analytic results for the relaxing stresses as shown below.

#### 3.2.1. Upstream layer

We suppose that the flow profile is simple shear with  $\chi = \frac{1}{2}\chi_u''(0)\xi^2$ . The evolution equations (17)–(19) may then be simplified by putting

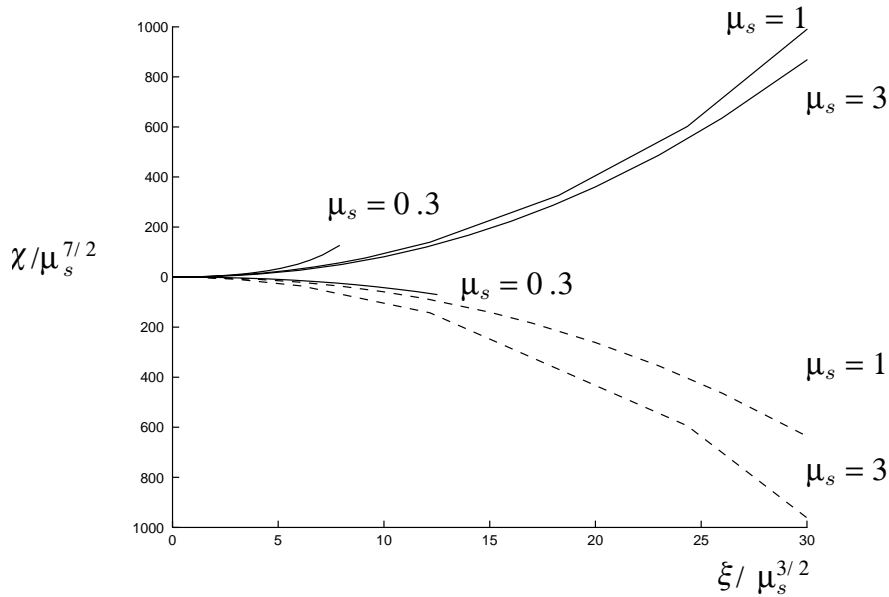


Fig. 8. Streamfunction  $\chi/\mu_s^{7/2}$  as a function of  $\xi/\mu_s^{3/2}$  for  $p = 2/3$ ,  $C = -0.2$  and values of  $\mu_s$  as shown. Continuous curves show the downstream layer; dashed curves are the upstream layer.

$$l = 2[\chi_u''(0)]^2 \hat{l}, \quad m = \chi_u''(0) \hat{m}, \quad n = \hat{n}, \quad \zeta = -\frac{1}{2}(3 - p)\chi_u''(0)\xi > 0, \tag{22}$$

to give

$$\begin{aligned} \zeta^2 \frac{d\hat{l}}{d\zeta} + [(1 - a)\zeta + 1]\hat{l} &= \hat{m}, & \zeta^2 \frac{d\hat{m}}{d\zeta} + [(1 - a)\zeta + 1]\hat{m} &= \hat{n}, \\ \zeta^2 \frac{d\hat{n}}{d\zeta} + [(1 - a)\zeta + 1]\hat{n} &= 1, \end{aligned}$$

with

$$a = \frac{1 + p}{3 - p} \quad \text{and} \quad \hat{l} = \hat{m} = \hat{n} = 1 \text{ at } \zeta = 0.$$

Rejecting the solutions of the form  $\zeta^{a-1}\exp(1/\zeta)$  that are unacceptable at the wall, we find

$$\begin{aligned} \hat{n} &= \zeta^{a-1} \exp\left(\frac{1}{\zeta}\right) \Gamma\left(a, \frac{1}{\zeta}\right), & \hat{m} &= \zeta^{a-1} \exp\left(\frac{1}{\zeta}\right) \left[ \Gamma\left(a + 1, \frac{1}{\zeta}\right) - \left(\frac{1}{\zeta}\right) \Gamma\left(a, \frac{1}{\zeta}\right) \right], \\ \hat{l} &= \zeta^{a-1} \exp\left(\frac{1}{\zeta}\right) \left[ \frac{1}{2} \Gamma\left(a + 2, \frac{1}{\zeta}\right) - \left(\frac{1}{\zeta}\right) \Gamma\left(a + 1, \frac{1}{\zeta}\right) + \left(\frac{1}{2\zeta^2}\right) \Gamma\left(a, \frac{1}{\zeta}\right) \right], \end{aligned}$$

where  $\Gamma(a, x)$  is an incomplete gamma function. We may then take the limit  $\zeta \rightarrow \infty$  to obtain

$$\lambda^* \rightarrow \frac{l}{(\chi')^2 |\chi|^{(2p-4)/(3-p)}} \rightarrow \Gamma(a + 2) \left[ -\frac{1}{2} \chi_u''(0) \right]^{2/(3-p)} (3 - p)^{-2(1-p)/(3-p)},$$

Table 1  
 Numerical and asymptotic results for the upstream boundary layer with  $p = 2/3$  and  $C = -0.05$

$\mu_s$	$\chi''_u(0)C$	$\mu^*/\lambda^*$	$v^*/\lambda^*$
1	0.250	1.167	3.04
10	0.224	1.167	3.18
30	0.221	1.167	3.22
100	0.219	1.167	3.25
$\infty$	0.218	1.167	3.27

with  $\Gamma(a)$  a complete gamma function. We find similarly that

$$\mu^* = \frac{(3 - p)\lambda^*}{2} \quad \text{and} \quad v^* = \frac{(3 - p)^2\lambda^*}{1 + p}.$$

We have thus determined the stresses throughout the shear region, including their asymptotic levels. Because the outer flow field is determined by these values via Eq. (14), it follows that

$$C = \frac{2}{(3 - p)^2} \left[ \Gamma\left(\frac{7 - p}{3 - p}\right) \right]^{-(3-p)/2} \frac{1}{\chi''_u(0)}, \tag{23}$$

and in particular for  $p = 2/3$ ,  $C = 0.218/\chi''_u(0)$ .

We conclude that provided  $\mu_s$  is sufficiently large it does not enter the relationship between  $C$  and  $\chi''_u(0)$ . Further, for the physical reasons discussed in Section 1, if the upstream wall shear rate is increased, the fluid velocity in the elastic core is reduced. Although this result has been derived in the limit  $\mu_s \rightarrow \infty$  with fixed  $C$  or  $\chi''_u(0)$ , in practice it works satisfactorily even for  $\mu_s = 1$  when  $C = -0.05$  as shown by the numerical results in Table 1.

A similar scaling behaviour for the upstream layer also applies whenever  $|\chi''_u(0)| \gg 1$  provided  $\mu_s$  remains of order unity. The flow profile near the wall is no longer linear, but stress relaxation occurs only within a small distance  $|\chi''_u(0)|^{-1}$  of the wall. Within this region the scalings (22) apply with  $\zeta = O(1)$ , and the flow satisfies Eq. (20) except that the pressure gradient  $1 - p$  is negligible so that the momentum equation becomes

$$\mu_s \chi''' - \frac{(3 - p)\chi l'}{\chi'} + \frac{(3 - p)\chi \chi'' l}{(\chi')^2} - (3 - 2p)l + m' = 0.$$

We do not have a closed form solution for this limit, but the scalings of  $\lambda^*$ ,  $\mu^*$ ,  $v^*$  and  $C$  with  $\chi''_u(0)$  apply as above. Numerical fits for  $p = 2/3$  and  $\mu_s = 1$  give the coefficients

$$C = \frac{0.25}{\chi''_u(0)}, \quad \frac{\mu^*}{\lambda^*} = 1.167, \quad \frac{v^*}{\lambda^*} = 3.00 \tag{24}$$

as  $|\chi''_u(0)| \rightarrow \infty$ , while for  $p = 2/3$  and  $\mu_s = 2$  these coefficients are 0.24, 1.167 and 3.05, respectively.

The result (23) is obtained on the basis that the flow in the wall region is simple shear. It therefore fails as  $\chi''_u(0) \rightarrow 0$ . Numerical results indicate that for fixed  $\mu_s$ ,  $|C|$  is a monotone decreasing function of the magnitude of the wall shear rate. Thus the fastest exterior flow rate is obtained when the wall shear rate vanishes. Results for these limiting flow rates are shown in Table 2.

Table 2

Numerical results for the maximum value of  $|C|$  in the upstream boundary layer with  $p = 2/3$  having zero shear rate on the wall

$\mu_s$	$C$
0.2	-0.41
1	-0.52
5	-0.81

Plots showing numerical values of  $\chi_u''(0)$  and  $\chi_d''(0)$  as functions of  $|C|$  for the case  $p = 2/3$  and  $\mu_s = 1$  are shown along with the scaling estimates in Fig. 9.

3.2.2. Downstream layer

If  $\mu_s$  is large, similar results may be developed for the stress in the downstream layer. The flow near the wall is  $\chi = \frac{1}{2}\chi_d''(0)\xi^2$ , and it is now appropriate to rescale the variables as

$$l = 2[\chi_d''(0)]^2 \hat{l}, \quad m = \chi_d''(0) \hat{m}, \quad n = \hat{n}, \quad \zeta = \frac{1}{2}(3 - p)\chi_d''(0)\xi > 0.$$

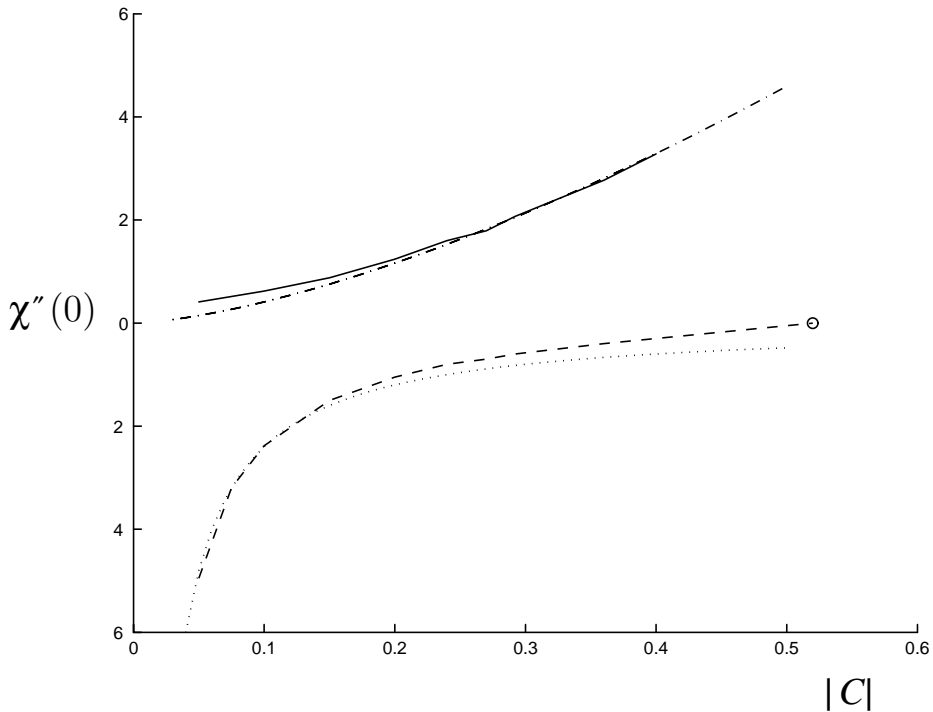


Fig. 9. Wall shear rates  $\chi_u''(0)$  and  $\chi_d''(0)$  as functions of  $|C|$  for  $p = 2/3$  and  $\mu_s = 1$ . Continuous curves show numerical results obtained for the downstream layer; dashed curves for the upstream layer.  $\circ$  shows the maximum possible value of  $|C|$  where  $\chi_u''(0) = 0$ . Asymptotes are (dotted)  $0.25/C$  from Eq. (24) and (dash-dot)  $13.0|C|^{3/2}$  from Eq. (21), with a numerical fit to the coefficient.

For simplicity, we present results for the stress  $\hat{n}$ , though we have developed analogous, more complicated expressions for  $\hat{m}$  and  $\hat{l}$ . It is straightforward to solve the equation for  $\hat{n}$  to obtain

$$\hat{n} = \zeta^{a-1} \exp\left(-\frac{1}{\zeta}\right) \left[ \int_{\zeta}^{\infty} y^{-a-1} \exp\left(\frac{1}{y}\right) dy + c_n \right],$$

where  $c_n$  is a constant whose value must be obtained by matching with the upstream stresses via  $v^*$ . Matching gives

$$c_n = \Gamma(a) \left[ -\frac{\chi_u''(0)}{\chi_d''(0)} \right]^{2/(3-p)}.$$

Expanding for the region close to the downstream wall  $\zeta \rightarrow 0$ , we find that

$$\hat{n} \rightarrow 1 - (a - 1)\zeta + \dots + c_n \zeta^{a-1} \exp\left(-\frac{1}{\zeta}\right).$$

This expression shows explicitly the essential singularity that vitiates a polynomial expansion near the downstream wall. The final term evidently has a maximum near  $\zeta = 1$ , where the stresses advected from infinity ‘pile up’ in the slow-moving fluid near the wall, see Fig. 5.

The scaling estimates of the previous section suggest that  $\chi_u''(0)$  remains of order unity as  $\mu_s \rightarrow \infty$ , whereas  $\chi_d''(0) \propto \mu_s^{(1-p)/p}$ , giving

$$c_n \propto \mu_s^{-2(1-p)/[p(3-p)]}.$$

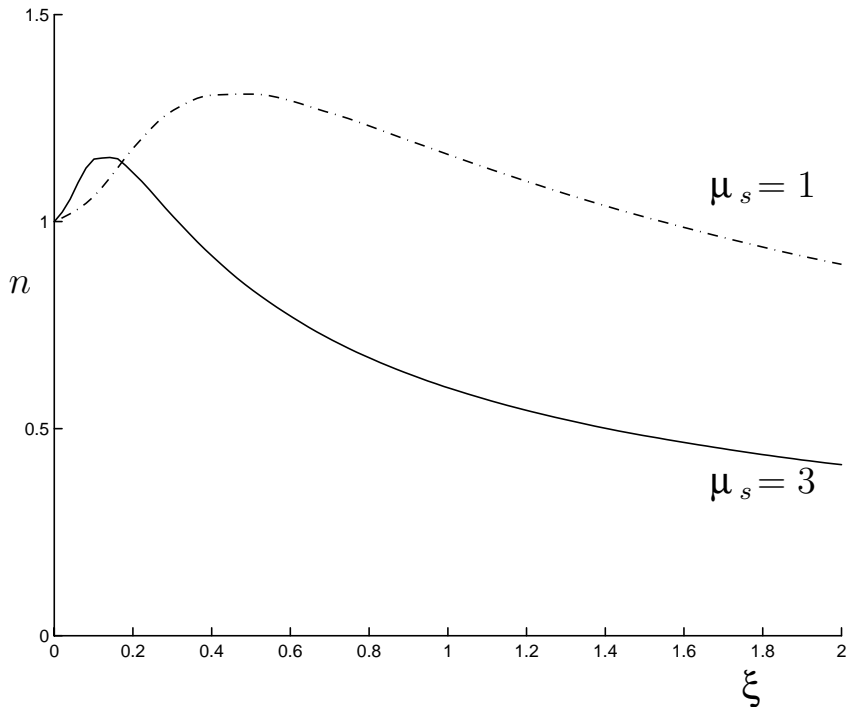


Fig. 10. Downstream elastic stresses  $n(\xi)$  for  $p = 2/3$ ,  $C = -0.2$  and  $\mu_s$  as shown.

Furthermore,  $\zeta = 1$  corresponds to  $\xi \propto \mu_s^{-(1-p)/p}$ . This suggests that the stress maximum in  $n$  will decrease and move toward the downstream wall as  $\mu_s$  is increased, consistent with the results in Fig. 10. Corresponding estimates may also be obtained for  $l$  and  $m$ .

In the Maxwell limit,  $\mu_s \rightarrow 0$ , computations become much more difficult. Our preliminary estimates (at any rate as far as  $\mu_s = 0.5$ ) suggest that the results converge to a finite limit as  $\mu_s \rightarrow 0$ .

#### 4. Conclusions

The principal result of this paper is to demonstrate for the first time the existence of a steady attached flow of an Oldroyd-B fluid near a reentrant corner of angle  $\pi/p$ . The stress near the corner has magnitude proportional to  $r^{2p-2}$ , and throughout most of the flow it is purely elastic, but near the walls there is a viscous stress of comparable magnitude. The streamfunction near the corner has magnitude proportional to  $r^{p(3-p)}$ . A remarkable feature is that for each corner angle and each viscosity there is a continuous one-parameter family of corner flows, so we are unable to specify a unique relationship between the stress and streamfunction near the corner. It is relatively straightforward to obtain satisfactory solutions for the upstream boundary layer, but difficult to do so for the downstream layer where relaxation methods are needed, and these converge slowly as the outer limit of integration is taken further from the wall.

Reverting to dimensional variables, we have shown that for any choice of the length-scale  $a$  there is a family of attached steady corner flows that have the form

$$\psi = \frac{a^2}{\tau} C \left(\frac{r}{a}\right)^{p(3-p)} \sin^{3-p}(p\theta); \quad P = -\frac{1}{2} G_e (1-p) \left(\frac{r}{a}\right)^{2p-2}, \quad (25)$$

for the streamfunction and pressure, respectively. The only restriction on this family is that for the flow to remain attached  $C < 0$  and for fixed  $\mu_s$  and  $p$  there is an upper limit to  $|C|$ .

A question that remains unresolved by our analysis is the selection mechanism within this family of singular corner flows that must operate in a finite geometry. As the family of steady solutions is *continuous*, every such flow must admit a neutrally stable perturbation on linear theory, so an analysis of the time-dependent problem cannot identify a unique stable flow.

A second possibility is that higher order boundary layer theory will impose an integrability constraint that will choose a particular solution at leading order. Such a constraint would putatively require that more than the leading order term in the outer velocity for each boundary layer must be matched across the core. We have explored this hypothesis to a limited extent. If, for example, we insist that the velocities should exactly match at the same finite distance  $\xi_\infty$  from each wall, then as we have already seen, for each choice of  $\xi_\infty$  there is a unique flow. The question is whether as  $\xi_\infty$  is increased without bound, a limiting value for  $C$  is obtained. The answer to this question, at any rate for  $p \leq 2/3$  is no, for the following reason.

The outer part of each boundary layer is controlled by the frozen stress equation (13). This equation has solutions for  $\xi \rightarrow \infty$  of the form

$$\chi = C \xi^{3-p} (1 + k(\xi)),$$

where

$$k(\xi) \propto \begin{cases} \xi^{2p-2}, & p > \frac{2}{3}, \\ \xi^{-2/3} \ln(\xi), & p = \frac{2}{3}, \\ \xi^{-p}, & p < \frac{2}{3}. \end{cases}$$

For  $p \leq 2/3$  the correction term is forced in (13) by the viscosity: it has the same sign for both the upstream and downstream layers. It is thus impossible to match both the leading order and correction terms in the velocity as  $\xi_\infty \rightarrow \infty$  for any fixed value of  $C$ . (If  $p > 2/3$  then the correction term is an eigensolution of (13), and thus matching as  $\xi_\infty \rightarrow \infty$  may be possible, but we have not explored this case.)

A final possibility that seems most plausible to us is that the choice of  $C$  is made by the outer flow, and is not a local property of the corner. For example the value of  $C$  at the reentrant corner formed by the junction between two channels might depend on the ratio of widths of the channels.

Some careful numerical work for the flow in a 4:1 contraction has been performed by Alves et al. [2] and by Aboubacar et al. [1]. At each Deborah number the steady flow is apparently unique. These authors have used highly refined meshes near the reentrant  $3\pi/2$  corner in order to identify the stress and flow singularities outside the boundary layers. For a steady attached flow, both groups find behaviours close to  $|\mu| \propto r^{5/9}$  and  $|\sigma| \propto r^{-2/3}$  near the corner as predicted.

In these computations, the overall flow rate is fixed and the polymer relaxation time  $\tau$  is progressively increased, thereby raising the Deborah number based on the downstream wall shear rate. The coefficients of the velocity and stress singularities are presented at only one value of  $\tau$  so we are unable directly to infer that different choices for  $C$  within the family (25) of attached corner flows are made. Nevertheless the results (e.g. those computed on the flow centreline) suggest that for flows that remain attached, the velocity near the corner is not substantially changed when  $\tau$  is doubled while the stress increases by about 20%. The scalings (25) then imply that as  $\tau$  is increased in the computations, so must  $|C|$ . Furthermore, at some critical value of  $\tau$  the computations no longer give an attached flow, corresponding, in our view to attainment of the maximum acceptable value for  $|C|$ . At that point, both authors find the appearance of a steady lip vortex upstream of the corner, and our analysis is no longer valid. We expect that the exponents of  $r$  for the streamfunction and stress will be altered in a separated flow; unfortunately no data are shown.

The computations of Aboubacar et al. [1], but not those of Alves et al. [2] suggest that steady separation may also occur on the downstream side of the corner. Our local analysis does not suggest, nor explain, such a phenomenon.

Analysis of the singular corner flow beyond separation is much more difficult because the flow history of material particles on the upstream side is complex. Computations indicate that flow inside the lip vortex is very weak. This implies that the effect of the vortex is to ‘flatten’ the angle of the reentrant corner, increasing the effective value of  $p$ . A stress balance along the separating streamline suggests further that along this streamline  $\chi''_u(0) = 0$ . This is certainly the condition at which flow separation first occurs and, as noted earlier, it corresponds for a given level of elastic stress, to the maximum possible value of  $|C|$  at the modified corner angle.

We therefore offer the following conjecture which, by analogy with inertial flows past aerofoils, might be called an elastic Kutta condition: when an elastic flow separates on the upstream side of a sharp reentrant corner, it does so at such angle  $\pi/p^*$  as makes  $\chi'' = 0$  on the separating streamline; outside the lip vortex, the corresponding flow near the corner is given by Eq. (25) with  $p = p^*$  and the largest possible value of  $|C| = |C^*|$ . These extreme values  $C^*(p^*, \mu_s)$  are plotted for three different values of  $\mu_s$  in Fig. 11.

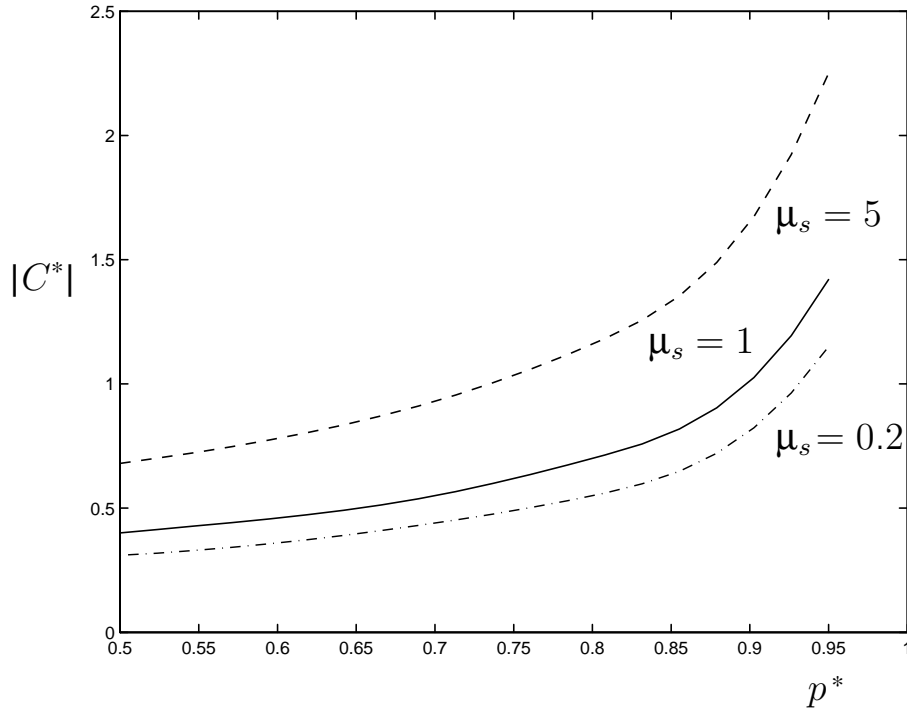


Fig. 11. Limiting values of  $|C^*|$  for corner angles  $\pi/p^*$  and  $\mu_s$  as shown.

A further question that arises is whether methods of the kind described here enable the determination of other singular steady flows of Maxwell/Oldroyd fluids. We think that the answer to this question is no; we have been unable to find by this technique the ‘stick-slip’ singularity (equivalent to a symmetric flow past a  $2\pi$  reentrant corner). The difficulty appears to be the satisfaction of the momentum equation along the slip streamline downstream of the stagnation point—just as it is for an extensional stagnation point; our contention is that no acceptable steady flow of a Maxwell/Oldroyd fluid exists in these geometries (see [5]).

## References

- [1] M. Aboubacar, H. Matallah, M.F. Webster, Highly elastic solutions for Oldroyd-B and Phan–Thien/Tanner fluids with a finite volume/element method: planar contraction flows, *J. Non-Newtonian Fluid Mech.* 103 (2002) 65–103.
- [2] M.A. Alves, P.J. Oliveira, F.T. Pinho, Benchmark solutions for the flow of Oldroyd-B and PTT fluids in planar contractions, *J. Non-Newtonian Fluid Mech.* 110 (2003) 45–75.
- [3] E.J. Hinch, The flow of an Oldroyd fluid around a sharp corner, *J. Non-Newtonian Fluid Mech.* 50 (1993) 161–171.
- [4] H.K. Moffatt, Viscous and resistive eddies near a sharp corner, *J. Fluid Mech.* 18 (1964) 11–18.
- [5] J.M. Rallison, E.J. Hinch, Do we understand the physics in the constitutive equation? *J. Non-Newtonian Fluid Mech.* 29 (1988) 37–55.
- [6] M. Renardy, How to integrate the upper convected Maxwell (UCM) stresses near a singularity (and maybe elsewhere too), *J. Non-Newtonian Fluid Mech.* 52 (1994) 91–95.
- [7] M. Renardy, A matched solution for corner flow of the upper convected Maxwell fluid, *J. Non-Newtonian Fluid Mech.* 58 (1995) 83–91.